

MACHINE PROTECTION CONSIDERATIONS FOR bERLinPro*

S. Wesch[†], M. Abo-Bakr, M. Dirsat, G. Klemz, P. Kuske, A. Neumann, J. Rahn, T. Schneegans
 Helmholtz-Zentrum Berlin, Berlin, Germany

Abstract

The Berlin energy-recovery-linac project bERLinPro at the HZB is a 50 MeV ERL test facility, which addresses physical and technological questions for future superconducting rf based high brightness, high current electron beam sources. The combination of a 100 mA cw beam, electron bunches with normalized emittances lower than $1 \text{ mm} \cdot \text{mrad}$ and the magnet optics of bERLinPro leads to power densities capable to harm the accelerator components within microseconds if total beam loss occurs. Furthermore, continuous beam loss on the level of 10^{-5} has to be controlled to avoid activation and to protect the SRF, beam diagnostics and other infrastructure components. In this paper, we present the evaluation of the required key parameters of the bERLinPro machine protection system and present its first conceptual design.

INTRODUCTION

bERLinPro [1, 2] is a single loop energy-recovery-linac (ERL) depicted schematically in Fig. 1. Generated in a SRF photo-injector, the cw 1.3 GHz electron beam is boosted to moderate beam energy, merged into the linac module and accelerated to the final energy. After 190 ns, the recirculator brings the beam back to the linac with a rf phase shift of π . Decelerated, it is separated from the concurrently accelerated high-energy beam in the splitter chicane and disposed into the beam dump. By the recovery of the expended energy, very intense and energetic beams of 100 mA can be produced with manageable overall power consumption. For bERLinPro the nominal beam parameters are listed in Table 1. In combination with a small average beam size of few hundreds of micrometers (down to $50 \mu\text{m}$ in both planes simultaneously), the beam power of "real" 650 kW at low energy and "virtual" 5 MW at high energy is able to damage the accelerator in a short time, hopefully prevented by an adequate machine protection system (MPS).

The MPS tasks are the detection of a beam loss, the processing of the raw signal and the creation of an inhibit trigger which interrupts the beam and ends the loss finally. For bERLinPro the simplest and most effective action is to shut-off or block the drive-laser such that no further electron bunches are produced. This is managed by the implemented fast pockels cells with response times of the order of 10 ns. Considering the traveling time of the remaining bunches of about 300 ns and an electronic signal transport with $2/3$ of the vacuum speed of light over ca. 100 m cable length, an intrinsic latency of $1 \mu\text{s}$ limits the MPS reaction time.

* Work supported by German Bundesministerium für Bildung und Forschung, Land Berlin, and grants of Helmholtz Association
[†] stephan.wesch@helmholtz-berlin.de

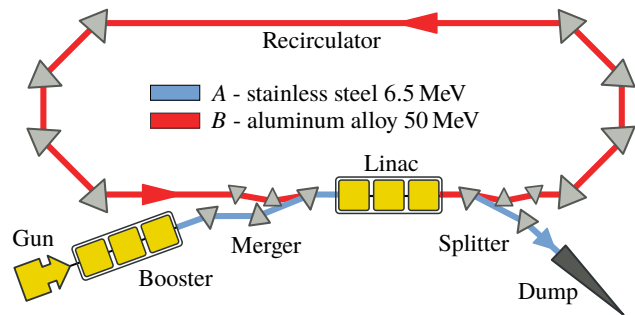


Figure 1: Schematic overview of bERLinPro.

So far and in contrast to user light source facilities, radiation sensitive insertion devices are not foreseen in bERLinPro. The MPS has to protect the accelerator structure, rf modules and diagnostics near the beam. We distinguish between permanent and total beam loss.

Permanent beam loss includes losses of a small fraction of the beam, mainly due to dark current and halo particles. Beside the activation of components and malfunction of nearby electronics, it can lead to local heating of structures causing vacuum leaks in the long run and - if the loss occurs in the recirculator - can hamper the energy-recovery limiting the maximum achievable beam current. The available linac rf power of 30 kW is sufficient to compensate for a current loss of 0.7 mA corresponding to a uniformly distributed loss of ca. $10 \mu\text{A/m}$. At 100 mA the relative beam loss has to be controlled locally to better than 10^{-4} .

Total beam loss refers to a full beam impact on any vacuum component. It can be caused by a breakdown of a device or an operating error. Due to the large beam power density a serious damage can happen on very short timescales compared to permanent beam loss. Not only a burn-through has to be avoided, but also evaporation from the wall surface which could lead to a contamination of the SRF cavities. In the following discussion of the MPS reaction time the permanent loss is not considered, but only the total beam loss.

Table 1: Nominal Beam Parameters of bERLinPro

Property	Value	Unit
Beam current I_{beam}	100	mA
Kinetic energy E_{kin}		
Gun	2.3	MeV
Injector/dump	6.5	MeV
Recirculator	50	MeV
Norm. trans. emittance ϵ_n	<1	mm · mrad
Avg. trans. beam size $\bar{\sigma}_{x,y}$		
Injector r.m.s.	0.5/0.5	mm
Recirculator r.m.s.	0.16/0.23	mm

TOTAL BEAM LOSS

The obvious damage caused by beam impact onto an accelerator structure is the melting of material. The time interval to do so can be treated as the required MPS detection and reaction time. For different situations, we have simulated the shower profile of a total beam loss and calculated the melting time of the material used for the chamber walls.

Up to moderate energies of 6.5 MeV the vacuum chamber is made mainly of stainless steel and the beam energy stays below the limit of photonuclear neutron production process [3]. This configuration is named setup A. At high energy of 50 MeV aluminum alloy is used for the recirculator, because the (γ, n) activation is reduced by one order of magnitude in comparison to stainless steel. It is called setup B in the following. Other energy-material-combinations, e.g. niobium cavities or higher order mode absorber ceramics are not examined in this report.

The beam itself can strike the vacuum pipe under various incident angles α_{in} describing the angle between the direction of the beam and the chamber surface: Grazing incidence on straight walls, moderate incidence at tapers and near normal incidence in the merger and splitter chicane.

Deposited Power

The deposited energy distributions for the different setups are calculated with FLUKA [4] taking reflected electrons and the escaping particle cascade into account. For the simulations the beam transverse shape is a round Gaussian profile with r.m.s. size of $\sigma_{beam} = 0.1$ mm. The following results are scaled to a current of 100 mA.

For three different angles, the volumetric power density \mathcal{P}_{vol} as a function of depth z is shown in Fig. 2. In case of normal impact for B the maximum power deposition is flat along the depth because of the large stopping power. The power density for setup A decreases by a factor of 5 over $\Delta z = 1$ mm. Along the narrow absorption channel the material is warmed up. At grazing incidence for both setups more than half of the power is deposited in the first 100 μ m of the chamber instantaneously heating a large area of the surface only.

The maximum power densities plotted against the incident angle are illustrated in Fig. 3. The power levels in both

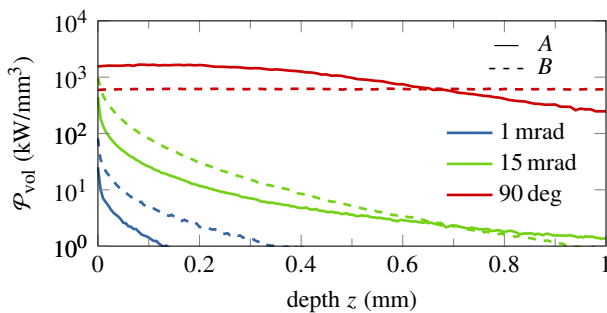


Figure 2: Penetration depth of absorbed power density at different angles for setup A and B.

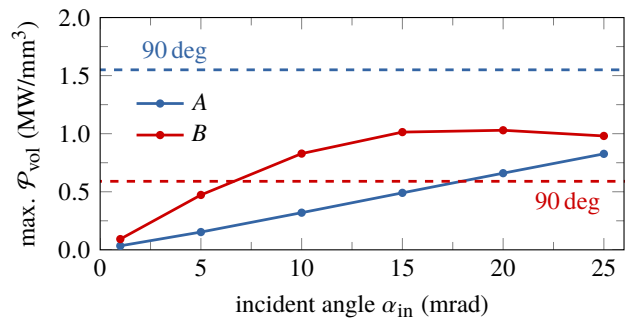


Figure 3: Incident dependent maximum deposited volumetric power density.

setups are comparable with densities used for electron beam welding of ca. 1 MW/mm^3 . Surprisingly for B, the maximum deposited power density around 20 mrad is larger than under normal incidence. It is caused the Bragg peak which is located near the surface.

Thermal Analysis

Before calculating the melting time, the time scale of effective heat transportation has to be estimated. Assuming a temperature-independent volumetric heat capacity of $c_{v,Al} = 2.4 \text{ J/cm}^3/\text{K}$ resp. $c_{v,steel} = 4.0 \text{ J/cm}^3/\text{K}$ and a thermal conduction of $\kappa_{Al} = 237 \text{ W/m/K}$ resp. $\kappa_{steel} = 16 \text{ W/m/K}$ the relaxation time of a sudden energy deposition can be evaluated. With the average beam sizes, see Table 1, and a two dimensional heat transport the half time of the maximum temperature is given by $t_{1/2} = \bar{\sigma}_{beam}^2 c_v / (2\pi\kappa)$. Because of the good thermal conductivity of aluminum $t_{1/2}$ is 65 μ s. In stainless steel it takes about 10 ms.

From the deposited power the time t_{melt} , which is needed to heat the surface up to the melting temperature

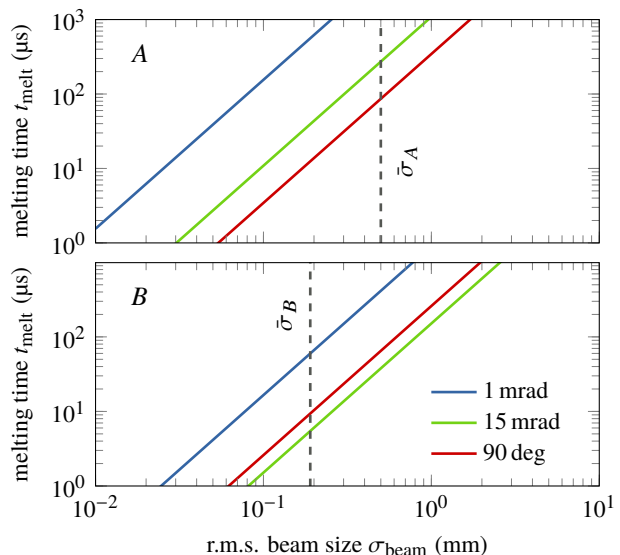


Figure 4: Beam size dependent melting times.

($T_{\text{melt,Al}} = 933 \text{ K}$ and $T_{\text{melt,steel}} = 1640 \text{ K}$), is statically calculated. The starting temperature is 300 K. The additional time buffer of the phase transition from the solid into the liquid state is neglected. In Fig. 4 these times as function of beam size are shown. The average beam sizes in the injector and recirculator are marked. The melting time for a high-energy beam is about 5 μs and for the low-energy beam 100 μs . First, these values are well below the estimated relaxation times and the heat conductivity is ineffective. Second, these times are a lower limit for the MPS by now.

MACHINE FAILURE EXAMPLES

The evaluated melting times are valid for a promptly and locally fixed error scenario. Considering hardware failures or operational errors, specific transition times until the machine is in a new fixed state has to be taken into account. Here we discuss three obvious failures neglecting special cavity dynamics.

Drive-Laser: A MPS relevant device is the 1.3 GHz photo-injector laser. It is planned as a soliton-mode-locked oscillator whose cw infrared pulses are converted by a non-linear birefringent crystal into a higher (2nd) harmonic. This type of laser oscillator can adapt oneself to stable operation with a double pulse structure inside one rf period. The phase shift is fixed, but can reach any phase value resulting in wrong electron beam energy, wrong focusing and an immediate beam loss. Assuming a pessimistic half-half split, the intensity of the phase-shifted electron beam reduces to one fourth by the non-linearity of the crystal and relaxes the MPS reaction time by the same amount.

Rf transmitter: Another main failure is a breakdown of an rf transmitter. Massive beam loading leads to a fast drainage of cavity field energy and an incorrect electron beam energy falling below the acceptance of bERLinPro. The fastest scenario is caused by a transmitter failure of one of the accelerating booster cavities. With a loss factor of 34.4 V per bunch ($Q = 77 \text{ pC}$) and an energy gain of $\Delta E_{\text{kin}} = 2.2 \text{ MeV}$ it takes 8.5 μs until the energy drops below the acceptance of the merger of 6 % and another 50 μs until the full energy is lost. In the latter case the beam is lost right after the first merger dipole under 160 mrad with $\sigma_{\text{beam}} \approx 1.3 \text{ mm}$. The melting time of A is relaxed about an order of magnitude, because the beam size increases by about a factor of three.

Magnets: In comparison to the short melting time, the change in magnet field strength takes rather long. Analog to BESSY II injector transfer line magnets, slew-rate-limiters damp the speed of setpoint errors ($\tau \approx 0.5 \text{ s}$), the field drop by a short circuit in the supply line is slowed due to the inductance (150 ms) and by a breaking cable in the coil slowed to 10 ms. In case of failures of quadrupole or solenoid magnets, the beam impacts the accelerator structure generally defocused which relaxes the situation. The failure of a corrector or dipole can be more harmful. On the one hand, these break-downs wipe the electron beam over the vacuum chamber and distribute the thermal load on a large area. But

on the other hand, if the duration is too long, the sweep under grazing incident might be too slow. Due to a longer melting time in low energy sections the situation is less critical compared to the high-energy recirculator. Here the combination of a field drop, the halt of energy-recovery and the decreasing beam energy (Linac stored energy collapsed within 90 μs with a loss factor of 366 V per bunch) may potentially pin the location of the loss. Loss scenarios are always accompanied with a loss of transmission to the dump. For the shortest time, which is needed to steer the beam onto the vacuum chamber at the linac exit, it is assumed that the most sensitive corrector is operated at full kick strength and that a short circuit provokes a field drop with $\tau \approx 10 \text{ ms}$. In at the most 0.75 ms the location of the beam loss travels from the dump to the linac exit. In case of a magnet error the MPS has to shut-off the laser during this time.

MPS DIAGNOSTICS

From the discussed considerations above, the loss detection, the processing, the triggering and the interrupt of operation have to take place in about conservative 100 μs . As a monitor of permanent beam loss a system of segmented ionization chambers are planned. Being sensitive on the slow moving ions created by the absorbed electrons the reaction time is in the order of milliseconds and they are not suitable for fast beam loss detection. Because of the limited budget other diagnostics suitable for a fast MPS are investigated.

- Distributed fast current transformers with a bandwidth of about 100 MHz
- Signals based on selected 1.3 GHz BPMs
- Rf signal cavity probes with ca. 80 MHz sampling [5]

All three monitors, especially monitors installed in the dump section, would guarantee the redundant detection of missing beam and could therefore lead to a safer operation.

CONCLUSION

The 100 mA electron beam of the bERLinPro test facility is capable to harm its components on the microsecond timescale based on analytical computation of the melting time of the vacuum chamber material under the assumption of total beam loss with the design optics. Including rf and beam diagnostics, the moderate response time of the foreseen ionization chambers could be overcome and one should be able to reduce the MPS reaction time down to the required range. First analysis of the failure scenarios suggest that overall reaction times of 100 μs are sufficient.

REFERENCES

- [1] J. Knobloch et al., ICFA Beam Dynamics Newsletters **58**, pp. 118–131, 2012.
- [2] M. Abo-Bakr et al., IPAC2014, MOPRO106.
- [3] K. Ott, M. Helmecke, IPAC2011, TUPO031, pp. 1503–1505.
- [4] G. Battistoni et al., AIP Conf. Proc. **896**, pp. 31–49, 2007.
- [5] J. Branlard et al., IPAC2012, MOOAC01, pp. 55–57.